SCIPEDIA Revista Internacional de Métodos Numéricos para Cálculo y Diseño en Ingeniería

Revista Internacional Métodos numéricos para cálculo y diseño en ingeniería RIMNI

In cooperation with CIMNE

Research on the Effects of Pit Excavation on Adjacent Existing Subway Tunnel Structures Based on the FEM-DEM Coupling Method

Donglin Meng[1,2], Wenkai Lei[1,*], Jingjing Han[1,3], Hao Li[4] and Yuanhua Huang[1]

[1]School of Architecture and Electrical Engineering, Hezhou University, Hezhou, 542899, China

[2]Guangxi Heyuan Technology Development Co., Ltd., Hezhou, 542899, China

[3]College of Civil Engineering and Architecture, Guangxi University, Nanning, 530004, China

[4]Shaanxi Dijian Land Comprehensive Development Co., Ltd., Xi'an, 710075, China

*Corresponding Author: Wenkai Lei. Email: llwwkk163@163.com

ABSTRACT

With the swift advancement of underground space development, large deep excavation projects above subway stations are becoming more common. This study employs the Finite element method-Discrete element method (FEM-DEM) coupling method to examine the effects of excavation on the structure of nearby subway tunnels. First, the flexible triaxial compression test was conducted using the FEM-DEM coupling method to acquire the macroscopic mechanical characteristics of various soil layers. Based on this, the ground particle model was developed using the particle size scaling method, the underground continuous wall support was constructed via the FEM-DEM coupling method, and the tunnel model was established using particles arranged circularly. The study shows that with the excavation, the particles at the bottom of the foundation start to heave upward, with the maximum uplift displacement being approximately 10 mm. Throughout the excavation process, substantial changes occur in the contact force chain within the pit, with notable stress release at the pit bottom. Moreover, the porosity at the pit bottom gradually increases, and the vertical stress decreases; the stress decreased by 75% compared to before excavation, primarily due to stress release during excavation. Lastly, a focused analysis was conducted on the tunnel deformation during excavation. Throughout the foundation pit excavation, the tunnel's displacement mainly took place within the excavation area, and its vertical displacement increased as the excavation depth increased, with a maximum displacement of approximately 0.5 mm. Analysis of particle displacement at various locations in the tunnel revealed that particles closest to the foundation pit bottom experienced the greatest displacement, whereas those farther away had relatively smaller displacements. The findings offer crucial theoretical support for the design and implementation of excavation projects.

OPEN ACCESS

Accepted: 16/10/2024

Submited: 27/08/2024

DOI
110.23967/
j.rimni.2024.10.57763

Keywords:
Excavation; FEM-DEM coupling; existing tunnels; force chain; stress release

1 Introduction

With the swift advancement of urban development, the underground rail transit network in cities is becoming increasingly dense. Concurrently, land development activities are continually seeking

space underground, resulting in frequent deep excavation projects across urban areas. The large-scale removal of original soil during the excavation of foundation pits causes additional stress and deformation in the surrounding soil. Consequently, urban subway tunnels are inevitably impacted by the excavation of foundation pits throughout their operational lifespan [1–3].

The influence of excavation on existing tunnels has long been a significant focus of research. Extensive studies have employed theoretical calculations [4–7], numerical modeling [8–12], and field monitoring [13–15] to investigate the uplift deformation phenomena of underlying subway tunnels during excavation. As urban construction and large-scale underground space development continue, projects involving excavation in proximity to existing tunnels are expected to become increasingly prevalent. Therefore, it is crucial to conduct more extensive research on these engineering projects.

To date, scholars both domestically and internationally have conducted substantial research on the effects of excavation on nearby existing tunnels [16–18]. In recent years, advancements in computing power and simulation software technology have enabled numerous studies to utilize numerical simulations to model foundation pits and tunnel structures. In finite element method (FEM), Zheng et al. [19] employed the finite element software and the ideal elastoplastic Mohr-Coulomb model to study, from both two-dimensional and three-dimensional perspectives, how excavation pits in soft soil layers affect the structure of tunnels located below the excavation surface and the surrounding soil. Similarly, Huang et al. [20] used the hardening soil model and finite element theory to analyze the three-dimensional deformation response of tunnels resulting from unloading during pit excavation, achieving outcomes concerning the range of influence on the structural response of the underlying tunnels due to the excavation. In discrete element method (DEM), Lei et al. [21] carried out a series of transparent soil model experiments to investigate the active face stability of the shield tunnel face adjacent to existing tunnels, focusing on development process, failure patterns, influence scope, and supporting forces. Zhou et al. [22] utilized physical model experiments and two-dimensional DEM analysis to investigate the deformation characteristics of existing tunnels structures due to unilateral excavation. The research indicates that unilateral excavation leads to the most pronounced lateral deformation at the station roof.

However, it must be pointed out that FEM is still applied to continuous media and does not adequately solve the problem of foundation soil particles being discontinuous media, leading to significant differences between simulation results and measured data. On the other hand, discrete element software has effectively solved the discontinuous media characteristics of soil particles, and as discussed earlier, its simulation results closely match the measured results [23]. Additionally, because discrete element software simulates each particle, it can more effectively investigate the meso-mechanisms of foundation pit deformation. However, it should be pointed out that since discrete element software started relatively late and has low visualization capabilities, along with a significant lack of corresponding secondary development, it is somewhat challenging to promote. Additionally, due to the limited numerical simulation research using discrete element software-particularly basic research-the relationship between simulation parameters and actual physical parameters remains relatively unclear, restricting the software's promotion and development.

Compared with previous studies, this paper offers the following innovations: (1) The paper is based on real engineering cases, and the calculation results are valuable for engineering applications. (2) The tunnel in this paper is constructed using a particle model, allowing for consideration of large tunnel deformations. (3) The foundation pit support is simulated using the FEM-DEM coupling method, enhancing the computational efficiency of the model.

This article investigates the deformation characteristics and damage evolution patterns of adjacent existing tunnels due to excavation. The study employed a FEM-DEM coupling approach. Initially, microparametric calibration of each stratum was conducted using triaxial compression tests with flexible boundaries. Subsequently, a FEM-DEM numerical model was developed to assess the impact of excavation on nearby existing tunnels. The analysis included both macroscopic and microscopic perspectives, examining stress fields, displacement fields, force chains, and porosity rates. These results provide valuable insights for engineering professionals in predicting risks for similar projects.

2 Engineering Overview

In this study, a pit excavation project adjacent to an existing subway tunnel is used as a case study. The maximum excavation depth is 8 m, performed in four stages, with 2 m excavated in each stage. The stratigraphic distribution within the excavation area consists of a clay layer on top and a gravel layer beneath. This foundation pit project utilizes a bored cast-in-place pile combined with an internal bracing support scheme. The cast-in-place piles have a diameter of 800 mm and a spacing of 1.1 m, with 600 mm diameter jet grouting piles used as an impermeable curtain between the piles. The existing tunnel beneath the pit has an internal diameter of 6 m, with the distance from the tunnel's top to the pit's bottom being about 8 m. The project overview is illustrated in Fig. 1.

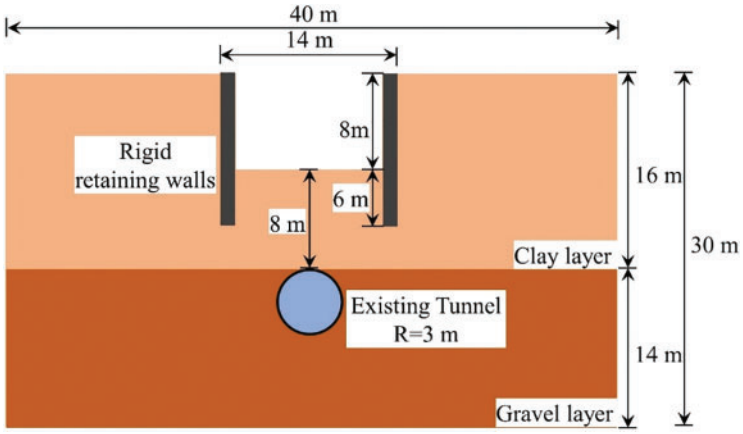

Figure 1: Project overview map

3 Calibration of Mesoscale Parameters for Carious Geological Layers

The macroscopic mechanical properties of the materials are governed by the microscopic parameters of the particles and the contact constitutive relationship in PFC. In this study, the FEM-DEM coupling method is employed to set up flexible triaxial compression tests to determine the macroscopic mechanical properties of various strata [24,25]. Shell elements are used as the lateral boundary conditions of the specimen in the triaxial test simulation. Unlike traditional rigid wall boundaries, the Shell model can represent the lateral deformation of the specimen during the loading process. The upper and lower boundaries are rigid wall boundaries. The schematic diagram of the flexible triaxial test is shown in Fig. 2a. Specifically, the clay layer uses a parallel bond model, while the gravel layer employs a rolling resistance model. The deviator stress-strain curves of the granular materials were obtained under confining pressures of 100, 200, and 300 kPa.

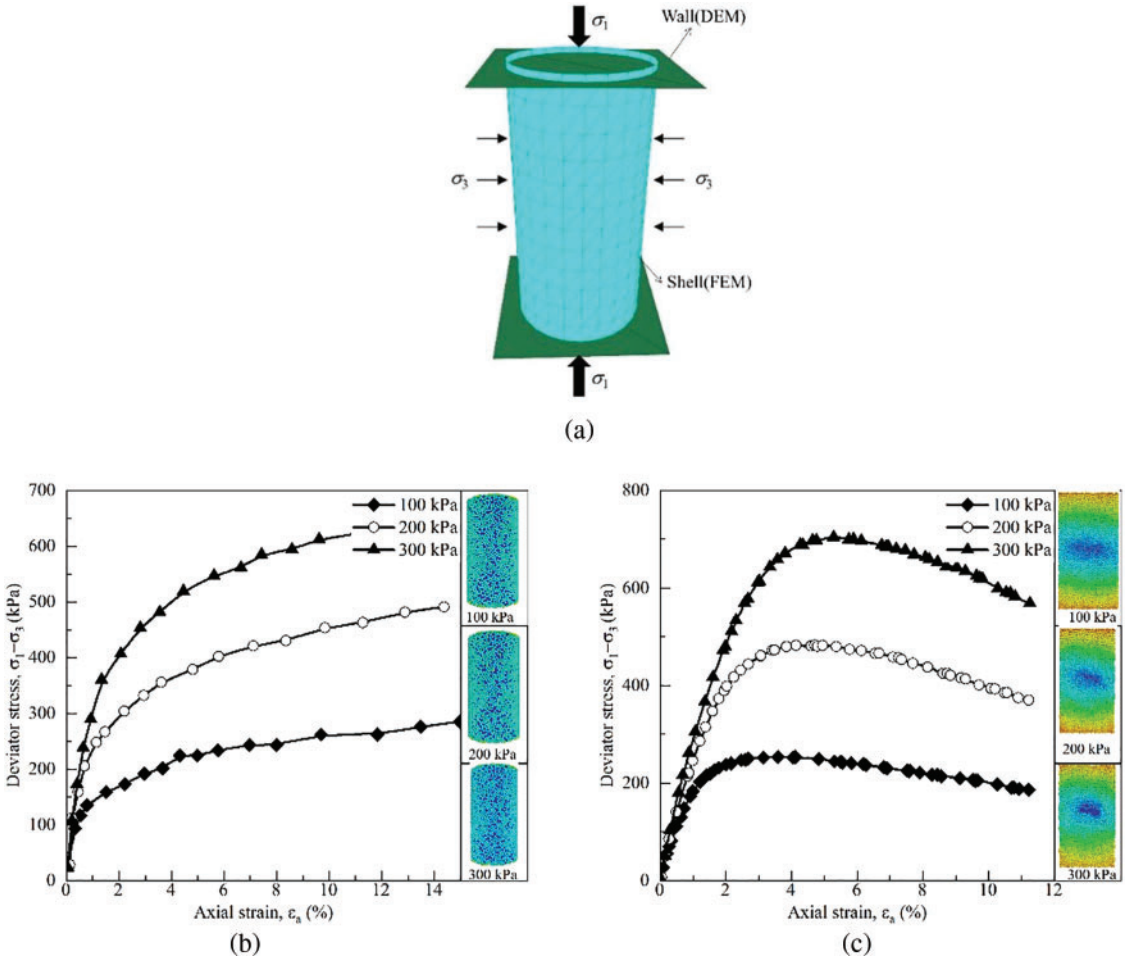

Figure 2: Calibration of mesoscale parameters. (a) Diagram of flexible triaxial compression experiment; (b) Stress-strain curve diagram for clay layers; (c) Stress-strain curve diagram for gravel layers

From Fig. 2, it is evident that the stress-strain relationships of different specimens in the triaxial compression tests show significant differences. The stress-strain curve of the clay layer indicates that with an increase in axial strain, the deviator stress gradually increases, displaying typical hardening characteristics. This suggests that in clay materials, as the strain increases, the contact force and friction between the internal particles intensify, leading to an improvement in load-bearing capacity. Experimental data indicate that under different confining pressures (100, 200, 300 kPa), the clay layer consistently shows a hardening trend. The maximum deviator stress increases with confining pressure, demonstrating that confining pressure significantly affects the load-bearing capacity of the clay layer.

In comparison, the stress-strain curve of the gravel layer shows noticeable softening characteristics. With the increase in axial strain, the deviator stress begins to decline after peaking, suggesting that in gravel materials, the contact force between particles decreases under high strain, leading to structural failure. Under varying confining pressures, the peak deviator stress of the gravel layer increases with rising confining pressure, but the post-peak rate of decline in deviator stress also accelerates. This indicates that the gravel layer is more susceptible to structural failure under high confining pressures.

4 Establishment of FEM-DEM Coupled Numerical Model

The foundation model consists of a series of three-dimensional particles. The particle diameter of the gravel layer is 0.5 m, with a particle count of 31,681. The particle diameter of the clay layer is 0.4 m, with a particle count of 72,000. Relevant foundation parameters are listed in Table 1. The numerical modeling process for the entire construction procedure, evaluating the impact of excavation on the existing tunnel structure, is as follows:

Table 1: Mesoscale parameters for various geological layers

Different strata	Clay	Gravel
Particle contact model	Linearpbond	Rrlinear
Effective modulus (Pa)	1×10^7	1×10^8
Normal-to-shear stiffness ratio	1	1
Bond effective modulus (Pa)	1×10^6	/
Bond normal-to-shear stiffness ratio	1	/
Tensile strength (N)	2.1×10^4	/
Cohesion (N)	2.1×10^4	/
Friction angle (°)	0	/
Friction coefficient	0.1	0.3
Rolling friction coefficient	/	0.1
Particle density (kg/m^{-3})	1650	2300

(1) Establish the model boundaries using rigid wall (Wall elements).

(2) ill within the model boundaries using Ball elements, compacting under self-weight. After multiple cycles, ultimately reach geostress equilibrium.

(3) Remove the soil particles in the tunnel cross-section area and generate a cluster of particles arranged in a circular ring. Use a parallel bond model between the particles. Compute until the system reaches equilibrium to simulate the tunnel excavation process.

(4) Remove the soil particles in the trench of the diaphragm wall and generate a Zone finite element model in the trench. Compute until system equilibrium is reached to simulate the construction of the diaphragm wall [26].

(5) The process of excavation is as follows: During excavation, remove the particles at the corresponding positions (ball delete command). Then, compute until the system reaches equilibrium or the ground displacement ceases. On this basis, proceed to the next stage of pit excavation. The complete modeling process is illustrated in Fig. 3.

The established model is illustrated in Fig. 4. The model comprises a clay layer and a gravel layer. In the model, the existing tunnel is generated with particles arranged in a circular ring. This method uses PFC to simulate the tunnel, precisely capturing the deformation characteristics during the excavation process. The circular ring arrangement of particles accurately simulates the tunnel's actual structure, resulting in higher simulation precision and effectively reflecting the tunnel's stress and deformation under various conditions.

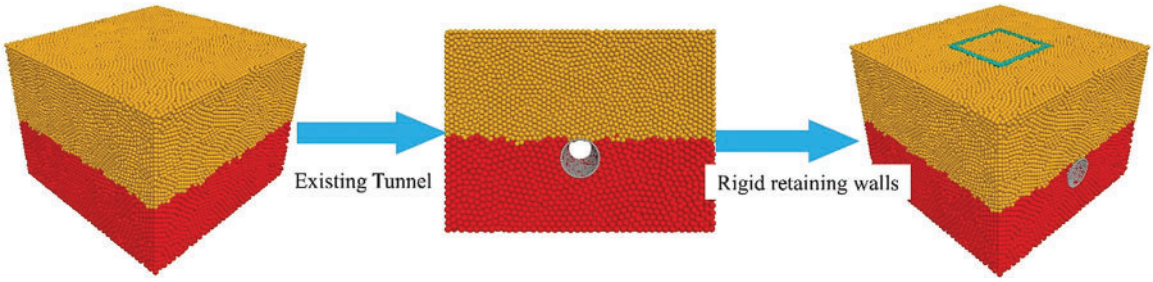

Figure 3: Process of establishing the excavation pit

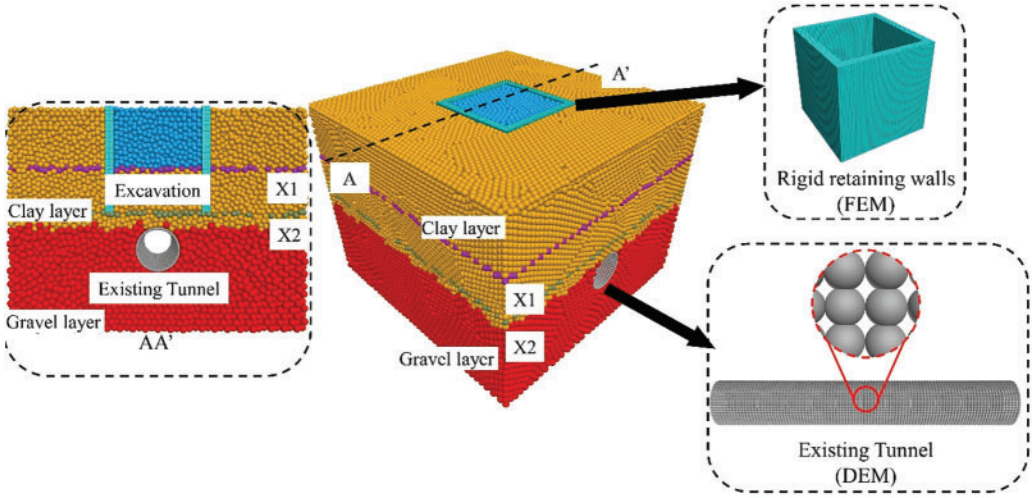

Figure 4: FEM-DEM coupled model for analyzing the impact of excavation on existing tunnels

A linear parallel bonding model is employed between particles in the tunnel. This model produces a certain displacement between particles under external loading. If the load surpasses the bond strength between particles, the particle bonds will fracture. Consequently, the model exhibits macroscopic failure.

Furthermore, the diaphragm walls (rigid retaining walls) are modeled using the Zone model in FLAC, a method that significantly improves the computational efficiency of the model. The finite element method offers substantial advantages in handling large-scale continuous media problems, allowing for rapid and accurate calculation of the forces and deformation of diaphragm walls during foundation pit excavation. In the model establishment process, the mechanical properties of various materials and structures were thoroughly considered. By integrating the strengths of FLAC and PFC, a comprehensive simulation of the foundation pit excavation process was achieved [27,28]. The model requires stress equilibrium after each excavation step. Once the maximum imbalance is less than 1e-5, carry out the next excavation step, continuing until the excavation is fully completed.

5 Analysis of Results

5.1 Foundation Displacement Field Analysis

The displacement contour map of pit is shown in Fig. 5. The color variations in the figure represent the magnitude of soil displacement at different stages, with blue to red indicating the displacement

magnitude from small to large. The figure shows that significant heave occurred at the base of the excavation pit, whereas the soil outside the pit did not experience noticeable displacement. As the excavation depth increases, the heave at the bottom of the pit also gradually increases, caused by pressure release. The displacement vectors of particles at the bottom of the foundation pit are predominantly vertical upward, particularly in the central area of the pit. This finding is consistent with the observed patterns in numerous cantilever-excavated foundation pits [29,30].

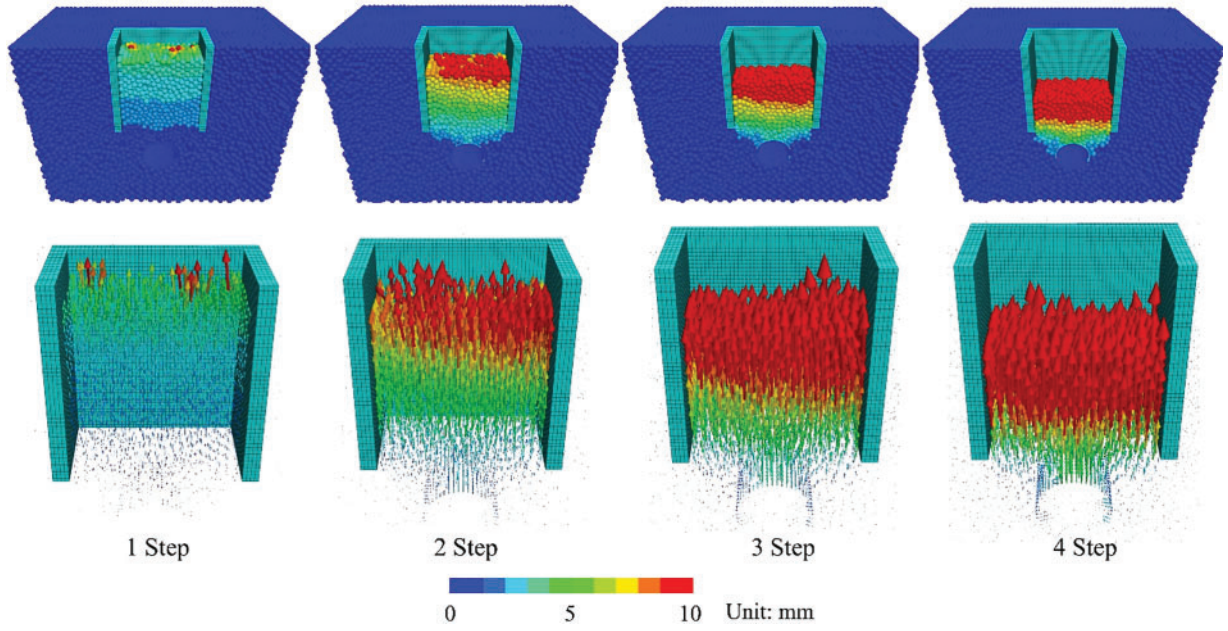

Figure 5: Excavation pit displacement contour map

Furthermore, the figure indicates vertical upward displacement in the area above the tunnel. This phenomenon is due to the redistribution of soil pressure above the tunnel caused by excavation, resulting in the upward movement of some soil. Detailed analysis: In the first step of excavation, initial heave has already occurred at the base of the pit, but the overall displacement is small. With the second step of excavation, the heave at the bottom of the pit increases significantly. The displacement vector diagram displays more vertical upward movement. By the 3 step of excavation, the heave at the bottom of the pit continues to increase, and the coverage area expands. As excavation pit progresses, the stress release in the soil at the bottom becomes more evident. Upon completion of the 4 step of the pit excavation, the heave at the bottom of the excavation pit reaches its maximum. The vector diagram of displacement shows that nearly the entire bottom of the pit is undergoing vertical upward movement, with the displacement being greatest at the center of the excavation pit.

Due to the excavation of the foundation pit, soil stress is redistributed, leading to upward deformation of the soil at the bottom, thereby causing uplift deformation of the pit. While it is usually hard to differentiate between pit uplift and bottom rebound, their mechanisms are quite straightforward in practical deformation scenarios. Soil rebound is unavoidable, as the unloading of soil from the pit top will naturally result in upward displacement, considered elastic deformation. Additionally, the uplift at the bottom can be categorized into elastic and plastic uplift. During the initial excavation phase, the pit bottom soil experiences elastic deformation, with the base uplift showing “small uplift at the sides and large uplift in the center.” Furthermore, the uplift of the soil

is influenced by the characteristics of the soil layers, the size of the pit, and factors like unloading load. At present, various methods exist for calculating pit bottom uplift deformation.

$$S_c = \psi_c \sum_{i=1}^{n} \frac{p_c}{E_{ci}} \left(z_i \bar{a}_i - z_{i-1} \bar{a}_{i-1}\right), \tag{1}$$

S_c–Amount of soil rebound at the pit bottom, mm; ψ_c–Empirical coefficient used in settlement calculations; p_c–Geostatic stress of soil below the base elevation, kPa; E_{ci}–Soil rebound amount.

5.2 Variation of the Displacement Field in the Particle Monitoring Layer

To gain a better understanding of the spatial variation characteristics of the foundation pit soil during excavation, two deformation monitoring layers (X1 and X2) were established in the model, as shown in Fig. 6. After the numerical calculations were completed, the displacement information of the particles in the Z direction was recorded, and the vertical displacement contour map was obtained through interpolation. The displacement contour map provides a clearer observation of the deformation patterns of the soil at the bottom and around the pit.

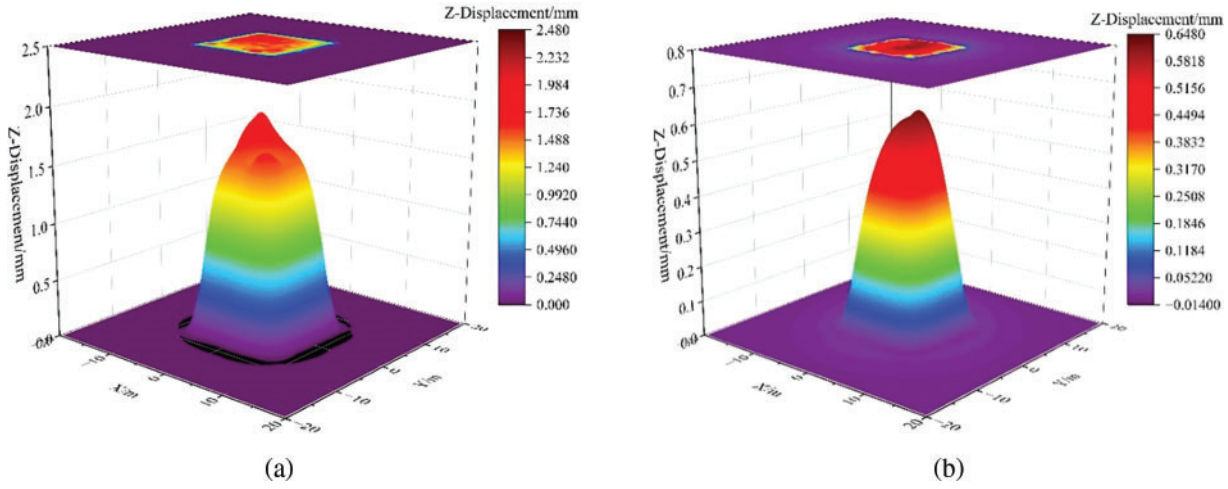

Figure 6: Monitoring layer final displacement cloud image. (a) X1 monitoring layer displacement cloud image; (b) X1 monitoring layer displacement cloud image

The figure reveals that the displacement of the monitoring layers is primarily characterized by heave, with this heave phenomenon being more pronounced near the central position. The heave has a shape close to conical, the vertical displacement of the soil exhibits a distribution pattern with larger displacement at the center and smaller displacement at the edges. This conical heave is primarily caused by the pressure release in the upper soil during the excavation process, resulting in the upward movement of the soil.

Specifically, the maximum displacement of the X1 monitoring layer is approximately 2 mm, while the maximum displacement of the X2 monitoring layer is around 0.65 mm. This result shows that the closer to the base of the pit, the greater the heave displacement of the soil. This is due to the soil of the pit undergoing significant vertical upward deformation as it bears the pressure release from the upper soil, resulting in an increase in the amount of heave.

Further analysis reveals that the X1 monitoring layer is located near the bottom, and thus is directly influenced by the excavation, leading to the largest displacement. In contrast, the X2 monitoring layer is located slightly farther from the pit and is therefore relatively less affected, resulting in smaller displacement. This phenomenon aligns with observations in actual engineering projects, indicating that displacement changes in the soil during excavation pit need to be closely monitored and analyzed to ensure the safety of the pit.

5.3 Force Chain Analysis

The DEM offers significant advantages in foundation engineering research, providing detailed data that traditional experimental methods find difficult to obtain. It is particularly suitable for analyzing the granular skeleton structure and force chain network. Fig. 7 illustrates the changes in particle contact force chains during the excavation, where the color of the lines indicates the relative magnitude of the contact forces. The distribution of force chains reveals that during the excavation, the force chains are sparse at the top and dense at the bottom. Specifically, the contact forces within the soil of the pit change significantly. The changes in the contact force chains at the bottom of the excavation pit are especially pronounced.

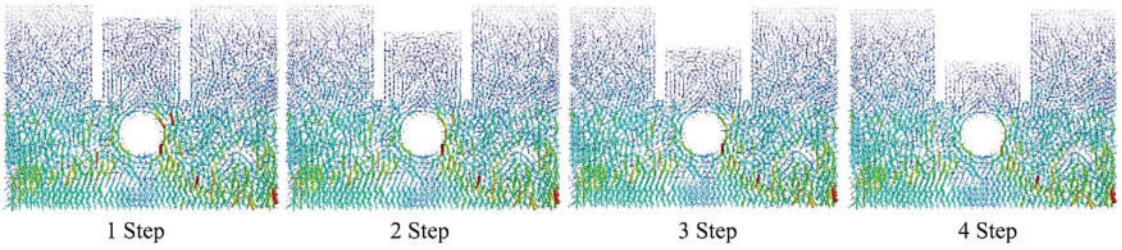

Figure 7: Analysis of force chains in the excavation pit process

As the excavation continues, the force chains at the base of the pit become sparser. This is primarily due to the upward movement of particles at the bottom of the pit during excavation, leading to stress release. Consequently, the contact between particles decreases, resulting in sparser force chains. Moreover, the distribution of force chains in the tunnel area also changes during the excavation process. The figure shows that the distribution of force chains in the tunnel area gradually diminishes as excavation advances. This is because the tunnel undergoes upward displacement during the excavation process, leading to stress release in the surrounding soil, which in turn reduces the contact forces in the tunnel area. This stress release not only reduces the contact forces around the tunnel but also lowers the overall structural strength of the tunnel.

The changes in force chain distribution indicate that stress release at the base of the excavation pit and in the tunnel area is a significant process during excavation. This stress release alters the contact force chains in the soil, thereby affecting the overall stability of the tunnel.

5.4 Analysis of Porosity and Stress Changes at the Bottom of the Excavation Pit

During the excavation, measurement circles (Fig. 8) are placed at the bottom of the pit to measure changes in porosity and vertical stress in Fig. 9 illustrates the variation patterns of porosity and vertical stress of the measurement spheres at different excavation steps. The figure shows that porosity gradually increases as excavation progresses. This is due to the stress release affecting the soil at the bottom of the excavation pit during excavation, causing the contacts between particles to loosen and thereby increasing the porosity. Specifically, during the 1 step of excavation, the porosity changes were

minimal, remaining relatively stable. However, beginning with the second step, the porosity showed a noticeable upward trend. During the third and fourth steps, the porosity increased further, indicating a gradual loosening process of the soil. Correspondingly, the vertical stress gradually decreases as the excavation progresses. In the first step of excavation, the vertical stress decreases slightly, but the change is not significant. In the 2 step of excavation, the vertical stress decreases significantly due to the reduction of overburden pressure on the soil at the bottom during excavation, resulting in stress release. During the 3 and 4 steps of excavation, the vertical stress continues to decrease, indicating that the stress release process at the bottom of the pit is ongoing. This phenomenon of increasing porosity and decreasing vertical stress indicates that the strength of the soil at the base gradually decreases during the excavation process. The increase in porosity reflects the loosening of the soil's internal structure, while the decrease in vertical stress indicates a reduction in the stress borne by the soil. Together, these factors lead to a gradual decrease in the strength of the soil. In summary, during the excavation, the porosity gradually increases with the excavation depth, while the vertical stress gradually decreases. These changes are primarily due to the stress release in the soil and the loosening of the particle structure during the excavation process.

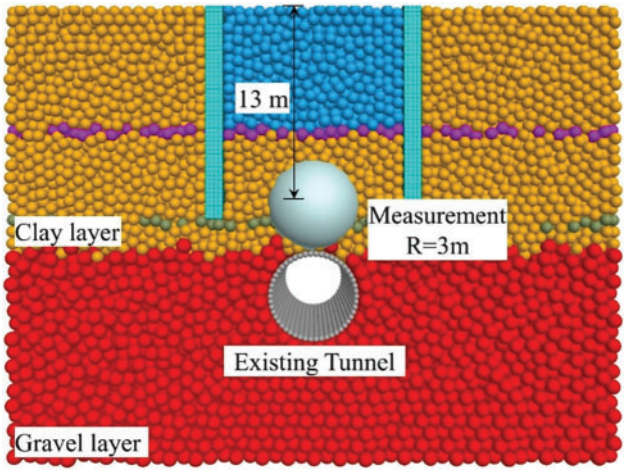

Figure 8: Location distribution of measurement spheres

5.5 Analysis of the Impact of Excavation Pit on the Deformation of Existing Tunnels

The excavation unloading of the pit will cause soil deformation, which will inevitably have a significant impact on the tunnel located beneath it. As shown in Fig. 10, as the pit is excavated, the tunnel gradually displaces upward. This upward displacement is due to the unloading caused by the excavation above the existing tunnel. Specifically, the maximum displacement of the tunnel occurs in the central area of the excavation pit, with the displacement direction being vertical upward, while the minimum displacement occurs near the ends of the tunnel.

In the 1 step of excavation, the tunnel deformation is relatively small and mainly concentrated in the central area. As the excavation progresses, the tunnel deformation gradually increases. During the 2 step of excavation, the upward displacement of the tunnel becomes more pronounced, with a noticeable increase in displacement. In the third and fourth steps of excavation, the upward displacement in the central area of the tunnel reaches its maximum, showing significant vertical upward deformation.

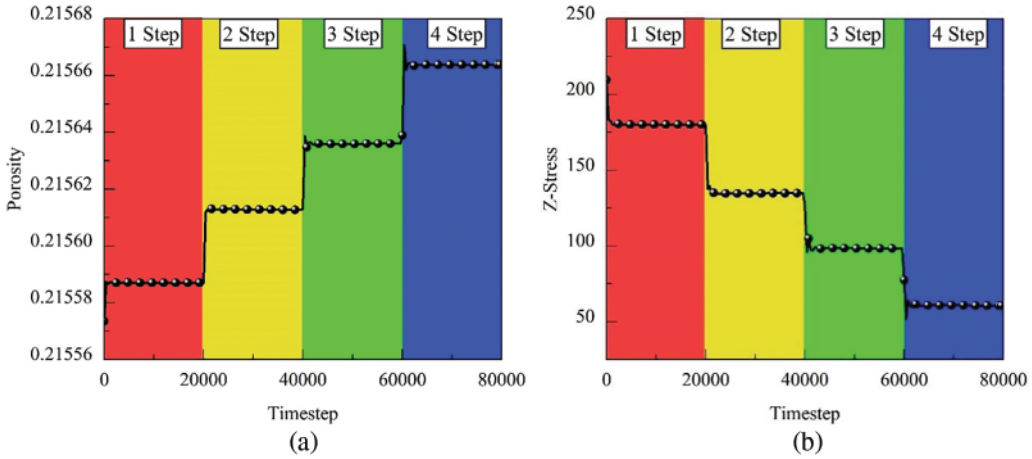

Figure 9: Curve of porosity and vertical stress changes at the bottom of the excavation. (a) Porosity change curve; (b) Vertical stress change curve

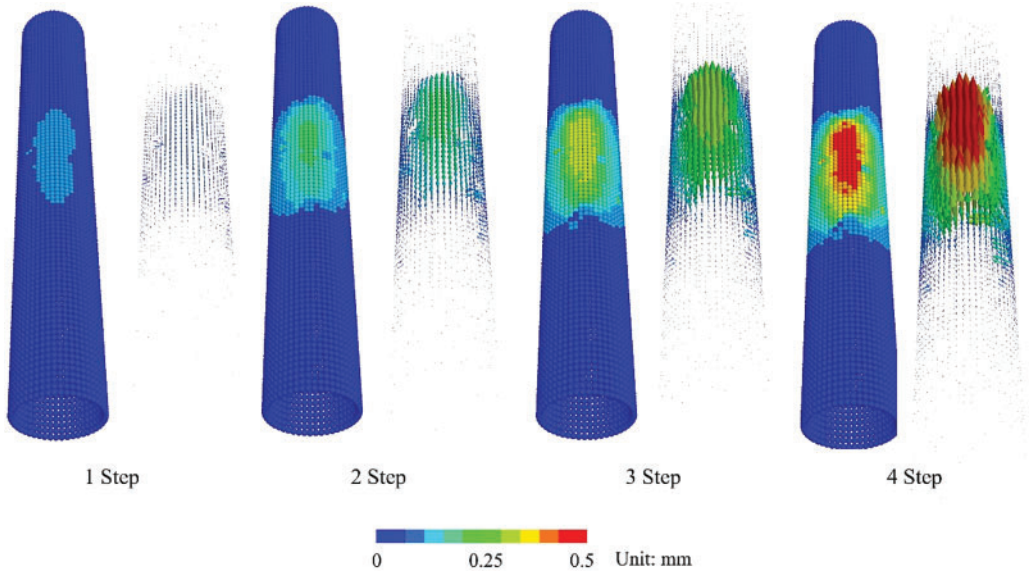

Figure 10: Displacement cloud map of tunnel deformation

This deformation can be explained by the redistribution of soil stress during the excavation. The excavation causes unloading of the overlying soil, and the pressure release results in upward movement, which in turn affects the deformation of the tunnel below. The central area of the tunnel, situated directly beneath the base, undergoes the greatest changes in overlying soil pressure, resulting in the largest vertical upward displacement. Conversely, the areas near the ends of the tunnel, being farther from the foundation pit, are relatively less affected and show smaller displacement.

This phenomenon suggests that in foundation pit excavation projects, special attention should be given to the deformation in the central area of the tunnel to ensure its structural safety. In summary, during the excavation, the tunnel's vertical displacement mainly occurs in the central area at the bottom of the pit, and the tunnel's displacement increases with the depth of the excavation.

The displacement of the particles at the top of the tunnel is extracted, and the particle distribution is illustrated in Fig. 11. The vertical displacement distribution of the tunnel at different steps is shown in Fig. 12. The figure shows that the heave displacement of the tunnel is mainly concentrated within the range of −7–7 m, corresponding to the excavation range of the pit. In the 1 step of excavation, the maximum displacement is approximately 0.08 mm. With the excavation depth increasing further, the vertical displacement of the tunnel continues to increase, ultimately reaching a maximum displacement of 0.5 mm during the fourth step of excavation.

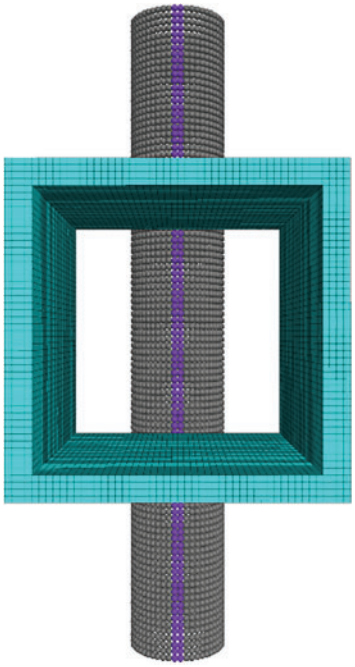

Figure 11: Particle distribution at the top of the tunnel

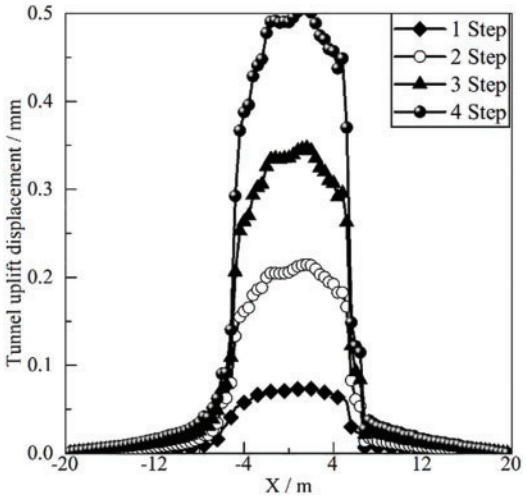

Figure 12: Displacement curves at the tunnel top for various excavation phases

The shape of the displacement curve in the figure shows that the displacement is greatest in the central area of the tunnel, gradually decreasing towards the sides, and eventually approaching zero at locations far from the excavation. In the initial stages of excavation, the increase in displacement is relatively slow. But as the excavation depth increases, the rate of displacement growth accelerates significantly. This indicates that the impact of excavation on the displacement of the tunnel exhibits distinct phase characteristics. Specifically:

Although the displacement of the tunnel increases with the excavation depth, the overall displacement is still significantly less than the heave displacement. This phenomenon indicates that while the excavation does affect the tunnel, this impact remains within a controllable range and has not caused excessive deformation of the tunnel.

In summary, the vertical displacement of the tunnel is mainly concentrated within the excavation area and increases gradually with each excavation step during the excavation. However, the overall displacement is significantly less than the heave displacement at the base of pit.

Prior to foundation pit construction, the tunnel is under force equilibrium. Since the soil's coefficient of earth pressure at rest $K0 < 1$, the horizontal principal stress acting on both sides of the tunnel is less than the vertical principal stress at the top, The tunnel's cross-section experiences "vertical compression and horizontal stretching" deformation, as illustrated in Fig. 13a. Following foundation pit construction, the stress acting above the tunnel becomes less than the horizontal stress, leading the tunnel's cross-section to transform into "vertical stretching and horizontal compression" [26], the tunnel's convergence deformation state is depicted in Fig. 13b.

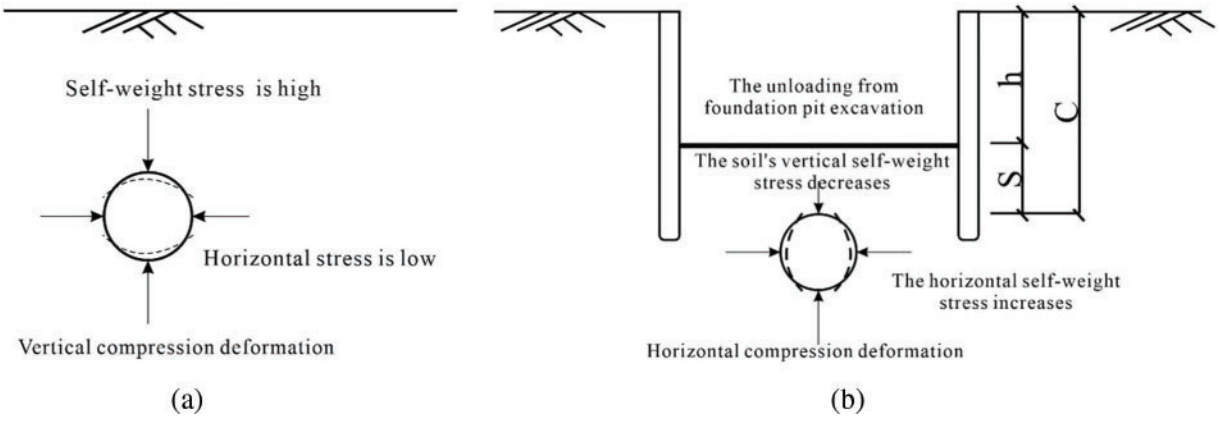

Figure 13: Deformation of the tunnel cross-section induced by foundation pit excavation. (a) Initial convergence state of the tunnel; (b) Tunnel convergence variation after foundation pit excavation

Fig. 14 illustrates the deformation shape of tunnel uplift along the longitudinal variation. After the overlying soil is removed, the rebound of the pit bottom leads to upward displacement of the tunnel. The maximum uplift of the tunnel is located at the center of the excavation and gradually diminishes toward both sides.

Fig. 15 shows the changes in vertical displacement of tunnel monitoring points under different conditions. For a detailed study, three representative particle positions within the tunnel are selected, where upward displacement of the tunnel is considered positive and downward displacement is negative. The figure indicates that with the increasing depth, the displacement of the tunnel also

increases. This suggests that the particles at the top of the tunnel move upwards, with the maximum displacement occurring in particles closest to the base of the excavation.

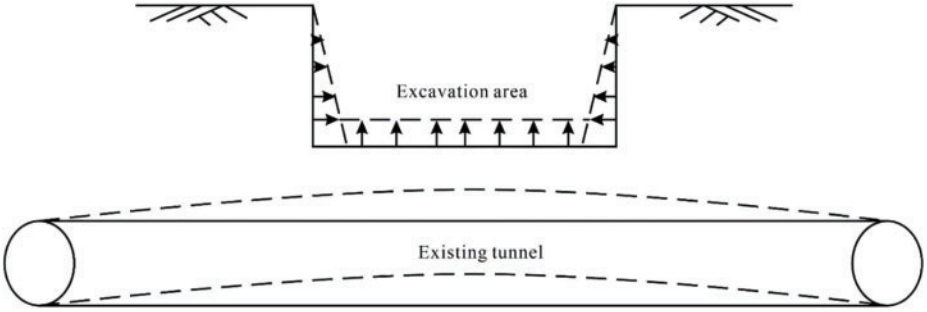

Figure 14: Longitudinal changes in tunnel uplift induced by pit excavation

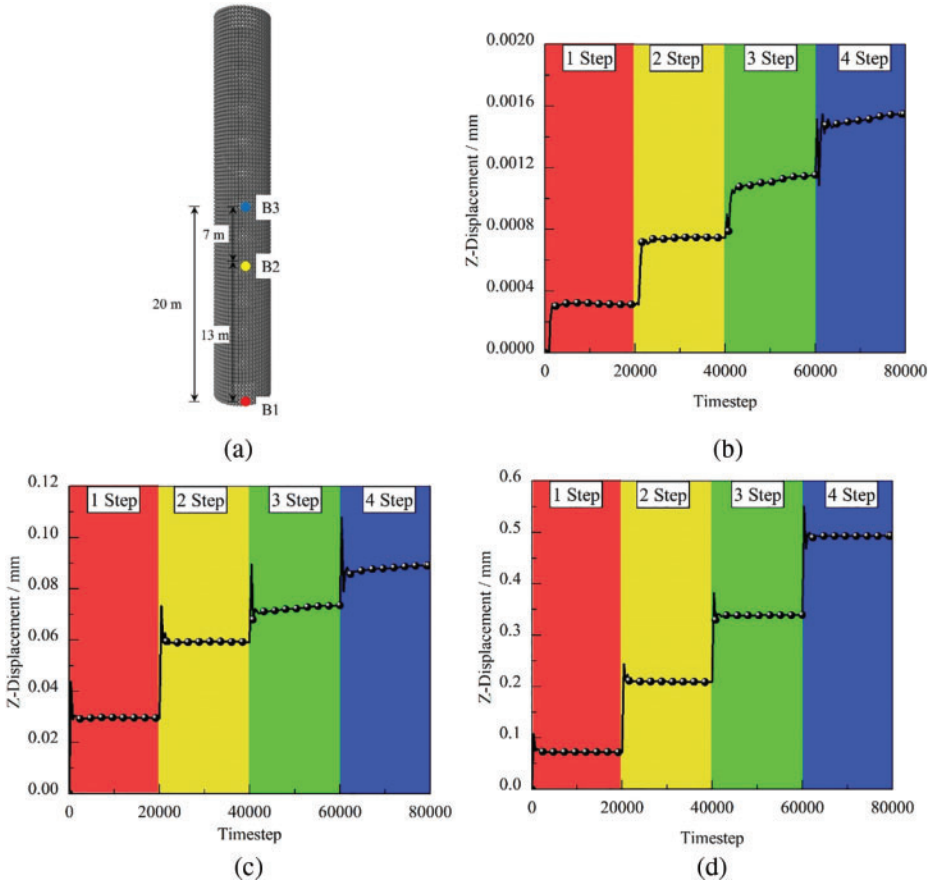

Figure 15: Displacement path analysis for particles at various positions. (a) Distribution of particle positions; (b) Displacement curve of B1 particles; (c) Displacement curve of B2 particles; (d) Displacement curve of B3 particles

In general, the vertical displacement at all monitoring points increases as the depth of excavation increases. Particles closer to the base of the excavation show the largest displacement, whereas those

further from the base exhibit relatively smaller displacements. This demonstrates that the effect of excavation on the particles at the top of the tunnel diminishes with distance. The step-like rise in the displacement curve indicates that each excavation step introduces new impacts on the tunnel particles, resulting in increased displacement.

By gathering 20 engineering cases in soft soil regions where foundation pit excavation impacts underlying tunnels, it was found that the vertical displacement of the tunnels was uplift in all cases, with maximum uplift amounts ranging between 0.4 and 15.9 mm, suggesting that the calculation results in this paper fall within a reasonable range for tunnel uplift.

6 Discussion

This paper merely takes into account the influence of foundation pit excavation in a simplified manner. In actual excavation processes, factors like pit dewatering, construction time, support methods, and subway operation conditions should be considered, all of which affect tunnel deformation to some extent. Although dewatering occurs during foundation pit excavation, this paper does not consider it due to the limitations of the discrete element method and concerns about computational efficiency. In future calculations, the fluid-solid coupling method can be employed to study the impact of pit excavation dewatering on existing tunnels. The findings of this paper have considerable theoretical significance regarding the deformation of tunnels following foundation pit excavation. The discrete element method excels in simulating soil failure, large deformation issues post-failure, and stress paths that are challenging to measure in practical engineering. While the discrete element method is currently unsuitable for practical engineering design, its analytical results regarding the mechanisms in foundation pit excavation processes are informative.

7 Conclusions

In this research, the FEM-DEM coupling method is employed to study the effects of pit excavation on the structure of adjacent existing metro tunnels. The conclusions are as follows:

The flexible triaxial compression test was conducted using the FEM-DEM coupling method to acquire the macroscopic mechanical characteristics of various soil layers. Then, the ground particle model was developed using the particle size scaling method. Based on this, the underground continuous wall support was constructed via the FEM-DEM coupling method, and the tunnel model was established using particles arranged circularly.

An obvious heave occurred at the bottom of the pit, whereas the soil outside the pit showed no significant displacement. With the increase of excavation depth, the bottom uplift of the foundation pit also gradually increases, reaching a maximum displacement of approximately 10 mm; this is due to stress release during the excavation. The displacement vectors of the particles at the pit bottom are predominantly upward, particularly in the central region of the pit where the particle displacement vectors are greatest.

The displacement of particles in the monitoring layer is primarily characterized by heave, with the heave shape approximating a cone, suggesting that the soil's vertical displacement exhibits a distribution pattern with larger displacement at the center and smaller at the edges. The nearer to the pit bottom, the greater the soil's uplift displacement.

In the excavation process, the contact forces within the pit soil change significantly. The variation of contact force chains at the bottom of the pit is especially evident. With the ongoing excavation, the

force chains at the pit bottom become sparser. This is primarily due to particles moving upward at the bottom of the pit during excavation, causing stress release.

The porosity increases progressively with the advancement of excavation. This occurs because stress release during the excavation process impacts the soil at the bottom of the pit, leading to loosened contacts between particles, which in turn increases the porosity. Throughout the excavation of the pit, the porosity at the bottom increases as the excavation depth increases, whereas the vertical stress decreases gradually. These variations are primarily caused by stress release in the soil and the loosening of particle arrangements during the excavation process.

The tunnel gradually moves upward with the excavation. This upward movement is caused by the unloading effect from the excavation above the tunnel. Specifically, the tunnel's maximum displacement occurs at the center of the excavation pit in a vertically upward direction, while the minimum displacement occurs near the tunnel ends. In the process of excavation, the tunnel's vertical displacement primarily occurs in the central area of the pit bottom, and it increases as the excavation depth increases. During the first excavation step, the tunnel's maximum displacement is around 0.08 mm; as excavation proceeds, the displacement keeps increasing, ultimately reaching about 0.5 mm at the fourth excavation step. The displacement is largest at the center of the tunnel, gradually lessening toward both sides, and eventually nearing zero at positions distant from the foundation pit excavation zone. Selecting three representative particle positions inside the tunnel, the displacement of the tunnel particles also increases as the excavation depth increases. The particles close to the foundation pit bottom show the greatest displacement, whereas those farther away display relatively smaller displacement.

In conclusion, this study has elucidated the mechanical behavior of different materials during foundation pit excavation and its effects on tunnel structures through detailed experiments and numerical simulations. The results offer significant theoretical support for the design and construction of foundation pit projects, assisting in the optimization of excavation plans to ensure the safety of tunnel structures.

Acknowledgement: This work was supported by the Guangxi Science and Technology Base and Talent Special Project. We gratefully acknowledge the Hezhou University and Shaanxi Dijian Land Comprehensive Development Co., Ltd., for providing the necessary equipment for this study. We would like to thank Dr. Zhang for his technical assistance during the experiments.

Funding Statement: This work had been supported by the Fund Project: Guangxi Science and Technology Base and Talent Special Project (No. Gui Ke AD23026035); Hezhou University Doctoral Research Start-Up Fund (No. HZUBS202207); Guangxi Natural Science Foundation of China (No. 2024GXNSFBA010173); The Hezhou Foundation for Research and Development of Science and Technology (Nos. 2024124, 2024125).

Author Contributions: The authors confirm contribution to the paper as follows: study conception and design: Donglin Meng, Wenkai Lei; data collection: Jingjing Han, Hao Li; analysis and interpretation of results: Donglin Meng, Wenkai Lei, Yuanhua Huang; draft manuscript preparation: Wenkai Lei, Yuanhua Huang. All authors reviewed the results and approved the final version of the manuscript.

Availability of Data and Materials: Due to the nature of this research, participants of this study did not agree for their data to be shared publicly, so supporting data is not available.

Ethics Approval: Not applicable.

Conflicts of Interest: The authors declare that they have no conflicts of interest to report regarding the present study.

References

1. Q. Sun, C. Yuan, and S. Zhao, "Numerical modeling of progressive damage and failure of tunnels deeply-buried in rock considering the strain-energy-density theory," *Rev. Int. Metod. Numer.*, vol. 40, no. 2, pp. 1–15, 2024. doi: 10.23967/j.rimni.2024.06.001.
2. W. Jiang, Y. Tan, J. Yan, Y. Ouyang, Z. Fu and Q. Feng, "A BP neural network-based micro particle parameters calibration and an energy criterion for the application of strength reduction method in MatDEM to evaluate 3D slope stability," *Rev. Int. Metod. Numer.*, vol. 39, no. 1, pp. 1–25, 2023. doi: 10.23967/j.rimni.2023.01.003.
3. P. Castaldo and M. De Iuliis, "Effects of deep excavation on seismic vulnerability of existing reinforced concrete framed structures," *Soil Dyn. Earthq. Eng.*, vol. 64, no. 3, pp. 102–112, Sep. 2014. doi: 10.1016/j.soildyn.2014.05.005.
4. X. Zhang, J. Yang, Y. Zhang, and Y. Gao, "Cause investigation of damages in existing building adjacent to foundation pit in construction," *Eng. Fail. Anal.*, vol. 83, no. 12, pp. 117–124, Jan. 2018. doi: 10.1016/j.engfailanal.2017.09.016.
5. S. Oztoprak, S. F. Cinicioglu, N. K. Oztorun, and C. Alhan, "Impact of neighbouring deep excavation on high-rise sun plaza building and its surrounding," *Eng. Fail. Anal.*, vol. 111, Apr. 2020, Art. no. 104495. doi: 10.1016/j.engfailanal.2020.104495.
6. M. N. Houhou, F. Emeriault, and A. Belounar, "Three-dimensional numerical back-analysis of a monitored deep excavation retained by strutted diaphragm walls," *Tunn. Undergr. Space Technol.*, vol. 83, no. 9, pp. 153–164, Jan. 2019. doi: 10.1016/j.tust.2018.09.013.
7. E. Miceli, D. Gino, and P. Castaldo, "Approaches to estimate global safety factors for reliability assessment of RC structures using non-linear numerical analyses," *Eng. Struct.*, vol. 311, no. 4, Jul. 2024, Art. no. 118193. doi: 10.1016/j.engstruct.2024.118193.
8. Z. Zhang, M. Huang, and W. Wang, "Evaluation of deformation response for adjacent tunnels due to soil unloading in excavation engineering," *Tunn. Undergr. Space Technol.*, vol. 38, no. 3, pp. 244–253, Sep. 2013. doi: 10.1016/j.tust.2013.07.002.
9. F. Huang, M. Zhang, F. Wang, T. H. Ling, and X. L. Yang, "The failure mechanism of surrounding rock around an existing shield tunnel induced by an adjacent excavation," *Comput. Geotech.*, vol. 117, no. S2, Jan. 2020, Art. no. 103236. doi: 10.1016/j.compgeo.2019.103236.
10. B. Liu, D. W. Zhang, C. Yang, and Q. B. Zhang, "Long-term performance of metro tunnels induced by adjacent large deep excavation and protective measures in Nanjing silty clay," *Tunn. Undergr. Space Technol.*, vol. 95, no. 3, Jan. 2020, Art. no. 103147. doi: 10.1016/j.tust.2019.103147.
11. F. Meng, R. Chen, H. Wu, S. W. Xie, and Y. Liu, "Observed behaviors of a long and deep excavation and collinear underlying tunnels in Shenzhen granite residual soil," *Tunn. Undergr. Space Technol.*, vol. 103, no. 6, Sep. 2020, Art. no. 103504. doi: 10.1016/j.tust.2020.103504.
12. D. M. Zhang, X. C. Xie, Z. L. Li, and J. Zhang, "Simplified analysis method for predicting the influence of deep excavation on existing tunnels," *Comput. Geotech.*, vol. 121, no. 2, May 2020, Art. no. 103477. doi: 10.1016/j.compgeo.2020.103477.
13. J. Zhang, R. Xie, and H. Zhang, "Mechanical response analysis of the buried pipeline due to adjacent foundation pit excavation," *Tunn. Undergr. Space Technol.*, vol. 78, no. 2, pp. 135–145, Aug. 2018. doi: 10.1016/j.tust.2018.04.026.

14. Y. Zhao, X. Chen, B. Hu, P. Wang, and W. Li, "Evolution of tunnel uplift induced by adjacent long and collinear excavation and an effective protective measure," *Tunn. Undergr. Space Technol.*, vol. 131, no. 1, Jan. 2023, Art. no. 104846. doi: 10.1016/j.tust.2022.104846.
15. Y. Zhao, X. Chen, B. Hu, L. Huang, G. Lu and H. Yao, "Automatic monitoring and control of excavation disturbance of an ultra-deep foundation pit extremely adjacent to metro tunnels," *Tunn. Undergr. Space Technol.*, vol. 142, Dec. 2023, Art. no. 105445. doi: 10.1016/j.tust.2023.105445.
16. R. Liang, T. Xia, M. Huang, and C. G. Lin, "Simplified analytical method for evaluating the effects of adjacent excavation on shield tunnel considering the shearing effect," *Comput. Geotech.*, vol. 81, no. 3, pp. 167–187, Jan. 2017. doi: 10.1016/j.compgeo.2016.08.017.
17. R. Z. Liang, W. B. Wu, F. Yu, G. S. Jiang, and J. W. Liu, "Simplified method for evaluating shield tunnel deformation due to adjacent excavation," *Tunn. Undergr. Space Technol.*, vol. 71, no. 4, pp. 94–105, Jan. 2018. doi: 10.1016/j.tust.2017.08.010.
18. G. Zheng, S. W. Wei, S. Y. Peng, Y. Diao, and C. W. W. Ng, "Centrifuge modeling of the influence of basement excavation on existing tunnels," in *Physical Modelling in Geotechnics*, 1st ed. London: CRC Press, 2010, pp. 523–527.
19. G. Zheng and S. W. Wei, "Numerical analyses of influence of overlying pit excavation on existing tunnels," *J. Cent. South Univ. Technol.*, vol. 15, no. S2, pp. 69–75, Apr. 2008. doi: 10.1007/s11771-008-0438-4.
20. X. Huang, H. F. Schweiger, and H. Huang, "Influence of deep excavations on nearby existing tunnels," *Int. J. Geomech.*, vol. 13, no. 2, pp. 170–180, Jan. 2013. doi: 10.1061/(ASCE)GM.1943-5622.0000188.
21. H. Lei, Y. Liu, Y. Hu, R. Jia, and Y. Zhang, "Active stability of the shield tunneling face crossing an adjacent existing tunnel: Transparent clay model test and DEM simulation," *Can. Geotech. J.*, vol. 60, no. 6, pp. 864–884, Apr. 2022. doi: 10.1139/cgj-2022-0294.
22. F. Zhou *et al.*, "Deformation characteristics and failure evolution process of the existing metro station under unilateral deep excavation," *Eng. Fail. Anal.*, vol. 131, no. 12, Jan. 2022, Art. no. 105870. doi: 10.1016/j.engfailanal.2021.105870.
23. F. Zarate, J. J. Cuellar, and M. J. M. Santana, "Saavedra Structural analysis of a railway bridge using the FEM-DEM technique," *Rev. Int. Metod. Numer.*, vol. 38, no. 1, pp. 1–17, 2022.
24. X. Zhang, M. Jiang, J. Yang, C. Zhao, and G. Mei, "The macroscopic and mesoscopic study on strengthening mechanisms of the single pile with raft under pile-soil-raft combined interaction," *Comput. Geotech.*, vol. 144, no. 4, Apr. 2022, Art. no. 104630. doi: 10.1016/j.compgeo.2021.104630.
25. X. Zhang, T. Wang, C. Zhao, M. Jiang, M. Xu and G. Mei, "Supporting mechanism of rigid-flexible composition retaining structure in sand ground using discrete element method," *Comput. Geotech.*, vol. 151, no. 3, Nov. 2022, Art. no. 104967. doi: 10.1016/j.compgeo.2022.104967.
26. H. Liu, G. H. Ma, and Z. Geng, "An improved FEM-DEM coupling simulation for granular-mediabased thin-wall elbow tube push-bending process," *Rev. Int. Metod. Numer.*, vol. 39, no. 2, pp. 1–9, 2023.
27. M. Dratt and A. Katterfeld, "Coupling of FEM and DEM simulations to consider dynamic deformations under particle load," *Granul. Matter*, vol. 19, no. 3, Nov. 2017, Art. no. 49. doi: 10.1007/s10035-017-0728-3.
28. H. Cheng, A. R. Thornton, S. Luding, A. L. Hazel, and T. Weinhart, "Concurrent multi-scale modeling of granular materials: Role of coarse-graining in FEM-DEM coupling," *Comput. Methods Appl. Mech. Eng.*, vol. 403, no. 5, Jan. 2023, Art. no. 115651. doi: 10.1016/j.cma.2022.115651.
29. M. Doležalová, "Tunnel complex unloaded by a deep excavation," *Comput. Geotech.*, vol. 28, no. 6, pp. 469–493, Oct. 2001. doi: 10.1016/S0266-352X(01)00005-2.
30. J. S. Sharma, A. M. Hefny, J. Zhao, and C. W. Chan, "Effect of large excavation on deformation of adjacent MRT tunnels," *Tunn. Undergr. Space Technol.*, vol. 16, no. 2, pp. 93–98, Apr. 2001. doi: 10.1016/S0886-7798(01)00033-5.